VII International Conference on Computational Methods for Coupled Problems in Science and Engineering
COUPLED PROBLEMS 2017
M. Papadrakakis, E. Oñate and B. Schrefler (Eds)

BOUNDARY ELEMENT ANALYSIS OF STEADY INCOMPRESSIBLE VISCOUS FLOW WITH ISOGEOMETRIC AND ISOPARAMETRIC DISCRETISATION

C. Duenser* and G. Beer*

* Institute for Structural Analysis
Graz University of Technology
Lessingstrasse 25/II, 8010 Graz, Austria
e-mail: duenser@tugraz.at
e-mail: gernot.beer@tugraz.at
web page: http://www.ifb.tugraz.at

Key words: BEM, isogeometric analysis, flow, incompressible

Abstract. In this work the boundary element method (BEM) is applied to steady incompressible viscous flow of Newtonian fluids. The boundary integral equation is derived from the continuity and momentum equation and the primary variables involved are velocity and traction. Due to the non-linearity of the governing differencial equation a volume integral arise in the formulation of the final equation system. Thus, iterative techniques, either a full or modified Newton-Raphson algorithm, are applied in the solution procedure.

The numerical discretisation is done in two different ways, firstly with the use of classical isoparametric continuous elements of linear and quadratic order. Using this type of elements geometry- and mesh-generation is a significant portion of the overall computation effort. In contrast to this, in a second implementation, the discretisation is done with the isogeometric analysis (IGA). With the IGA geometry data can be taken directly from Computer Aided Design (CAD) programs, potentially eliminating the need for mesh generation. The arising surface and volume integrals of the BEM are evaluated with both techniques, the isoparametric application and with the IGA.

Computational results are shown for the two different numerical implementations based on a 2D benchmark example. The accuracy of the results of both methods are compared as well as the computational effort, such as numbers of degrees of freedom and internal point calculations.

1 INTRODUCTION

For the solution of viscous flow problems in many publications domain methods such as the Finite Difference, Finite Elements or Finite Volumes are used. A widely used benchmark example is the forced flow in a cavity and very accurate results are available with a solution of a very fine finite difference discretisation by [1].

In this work we use the Boundary Element Method (BEM). The discretisation is done with the classical isoparametric analysis and with the isogeometric analysis (IGA) [2]. With IGA geometry data can be taken directly from Computer Aided Design (CAD) programs [3], potentially eliminating the need for mesh generation. With the BEM for linear problems unknowns only exist at the domain boundary and the solution inside the domain satisfies the governing differential equation. For the present non-linear problem volume integrals arise.

2 THE BOUNDARY ELEMENT METHOD - BASIC FORMULATION

The laws of conservation of mass and momentum are the basis for the differential equations for steady incompressible flow which are written in the form:

$$\frac{\partial u_j}{\partial x_j} = 0 \qquad \mu \frac{\partial^2 u_i}{\partial x_j \partial x_j} - \frac{\partial p}{\partial x_i} - \rho u_j \frac{\partial u_i}{\partial x_j} = 0 \tag{1}$$

where x_i is the Eulerian coordinate, u_i is the velocity vector, p is the pressure, ρ the mass density and μ the viscosity. The non-linear Equation (1) is considered by the BEM by treating the non-linear terms as body forces. Thus, Equation (1) is reformulated as:

$$\frac{\partial u_j}{\partial x_j} = 0 \qquad \mu \frac{\partial^2 u_i}{\partial x_j \partial x_j} - \frac{\partial p}{\partial x_i} + f_i = 0 \tag{2}$$

with

$$f_i = -\rho u_j \frac{\partial u_i}{\partial x_j} \tag{3}$$

We define fluid stresses as:

$$\sigma_{ij} = \mu \left(\frac{\partial u_i}{\partial x_j} + \frac{\partial u_j}{\partial x_i} \right) \tag{4}$$

and the resulting tractions on boundary S:

$$t_i = \sigma_{ij}\, n_j - p\, n_i \tag{5}$$

where n_i is the unit vector normal to the boundary. Using the reciprocal theorem, the following integral equation is obtained (for a full derivation we refer to [4]):

$$c_{ij}(y)\, \dot{u}_j(y) = \int_S \left[U_{ij}(y,x)\, t_j(x) - T_{ij}(y,x)\, \dot{u}_j(x) \right] dS(x) + \int_{V_0} U_{ij}(y,\bar{x})\, f_j(\bar{x}) dV_0(\bar{x}) \tag{6}$$

where $c_{ij}(y)$ is an integral free term, depending on the shape of the boundary and $\dot{u}_i$ is the velocity perturbation, i.e. the total velocity can be written as:

$$u_i(x) = \dot{u}_i(x) + u_i^0(x) \tag{7}$$

where u_i^0 is the free stream velocity and $U_{ij}(y,x)$ and $T_{ij}(y,x)$ are fundamental solutions for the velocity and traction at point x due to a source at point y.

In Equation (6) f_j appears involving derivatives of velocities. As has been shown in [5] these derivatives can be computed by using finite differences or by taking derivatives of an approximation of the velocity field. In both cases additional computational work needs to be done and errors are introduced.

Alternatively, the requirement of computing derivatives can be eliminated by applying the divergence theorem to the volume integral in Equation (6) resulting in:

$$\begin{aligned} c_{ij}(y)\,\dot{u}_j(y) = &\int_S \left[U_{ij}(y,x)\,t_j(x) - T_{ij}(y,x)\,\dot{u}_j(x)\right] dS \\ &- \int_{S_0} U_{ij}(y,x)\,t_j^0(x) dS_0 + \int_{V_0} U_{ij,k}(y,\bar{x})\,b_{jk}^0(\bar{x}) dV_0 \end{aligned} \tag{8}$$

where $U_{ij,k}(y,x)$ is a derived fundamental solution and:

$$\begin{aligned} b_{ik}^0(\bar{x}) &= \rho\,u_k(\bar{x})\,\dot{u}_i(\bar{x}) \\ t_i^0(x) &= b_{ik}^0(x)\,n_k(x) \end{aligned} \tag{9}$$

3 ISOPARAMETRIC DISCRETISATION

As in the work of [4] for the surface discretisation Lagrangian elements of linear or parabolic order are used to approximate the geometry and the boundary unknowns u and t. For the volume integral in Equation (8) cells are used to evaluate the integral.

3.1 Discretisation - Equation system

We use the collocation method, i.e. we write the integral equations for a finite number (N) of source points at locations $\mathbf{y}_n$. Changing to matrix notation, the integral equations are re-written as:

$$\begin{aligned} \mathbf{c}\left(\mathbf{y}_n\right)\,\dot{\mathbf{u}}\left(\mathbf{y}_n\right) = &\int_S \mathbf{U}\left(\mathbf{y}_n,\mathbf{x}\right)\mathbf{t}\left(\mathbf{x}\right)\mathrm{d}\,S - \int_S \mathbf{T}\left(\mathbf{y}_n,\mathbf{x}\right)\dot{\mathbf{u}}\left(\mathbf{x}\right)\mathrm{d}\,S \\ &- \int_{S_0} \mathbf{U}\left(\mathbf{y}_n,\mathbf{x}\right)\mathbf{t}_0\left(\mathbf{x}\right)\mathrm{d}\,S_0 + \int_{V_0} \mathbf{U}'\left(\mathbf{y}_n,\bar{\mathbf{x}}\right)\mathbf{b}_0\left(\bar{\mathbf{x}}\right)\mathrm{d}\,V_0 \end{aligned} \tag{10}$$

with $n = \{1,\ldots,N\}$. In the above $\mathbf{c}\left(\mathbf{y}_n\right)$ is a matrix containing integral free terms, $\dot{\mathbf{u}}(\mathbf{x})$ and $\mathbf{t}(\mathbf{x})$ are vectors containing perturbation velocities and tractions at point $\mathbf{x}$

on the boundary. $\mathbf{U}(\mathbf{y}_n, \mathbf{x})$ and $\mathbf{T}(\mathbf{y}_n, \mathbf{x})$ are matrices containing fundamental solutions described in [4]. $\mathbf{b}_0(\bar{\mathbf{x}})$ is a body force vector at a point $\bar{\mathbf{x}}$ inside V_0.

For the discretisation of the surface integrals over S the boundary is divided into elements and we apply the isoparametric concept where the same basis functions are used for the approximation of the geometry and the field values.

$$\mathbf{x}^e = \sum_{k=1}^{K} N_k(\xi)\, \mathbf{x}_k^e \qquad \dot{\mathbf{u}}^e = \sum_{k=1}^{K} N_k(\xi)\, \dot{\mathbf{u}}_k^e \qquad \mathbf{t}^e = \sum_{k=1}^{K} N_k(\xi)\, \mathbf{t}_k^e \tag{11}$$

In the above equations the superscript e refers to the number of the element, N_k are element basis functions with respect to the local coordinate ξ for the geometry, velocities and tractions respectively. $\mathbf{x}_k^e$ specify the location of the element nodes and $\dot{\mathbf{u}}_k^e$ and $\mathbf{t}_k^e$ are the parameters for velocities and tractions associated to the node k. K are the number of parameters depending on the order of basis functions (linear or quadratic) for each element.

Inserting the approximations into the integral equations the following discretised integral equations are obtained:

$$\sum_{e=1}^{E}\sum_{k=1}^{K} \triangle\mathbf{U}_{nk}^e \mathbf{t}_k^e = \sum_{e=1}^{E}\sum_{k=1}^{K} \triangle\mathbf{T}_{nk}^e \dot{\mathbf{u}}_k^e + \sum_{e=1}^{E}\sum_{k=1}^{K} \triangle\mathbf{U}_{nk}^e \mathbf{t}_{0k}^e - \sum_{c=1}^{C}\sum_{k=1}^{K} \triangle\mathbf{U'}_{nk}^c \mathbf{b}_{0k}^c \tag{12}$$

Furthermore

$$\triangle\mathbf{U}_{nk}^e = \int_{-1}^{1} \mathbf{U}\left(\mathbf{y}_n, \mathbf{x}^e(\xi)\right) N_k(\xi)\, J\, \mathrm{d}\,\xi \tag{13}$$

$$\triangle\mathbf{T}_{nk}^e = \int_{-1}^{1} \mathbf{T}\left(\mathbf{y}_n, \mathbf{x}^e(\xi)\right) \cdot N_k(\xi)\, J\, \mathrm{d}\,\xi$$

$$\triangle\mathbf{U'}_{nk}^c = \int_{-1}^{1}\int_{-1}^{1} \mathbf{U'}\left(\mathbf{y}_n, \mathbf{x}^e(\xi,\eta)\right) N_k(\xi,\eta)\, J\, \mathrm{d}\,\xi\, \mathrm{d}\,\eta$$

In the above J is the Jacobian of the transformation from local ξ to global (x, y) coordinate systems. The integral free term together with the strongly singular integral term of Equation (10) is evaluated using the rigid body motion shown in [6]. After assembly the following system of equations

$$[\mathbf{U}]\{\mathbf{t}\} = [\mathbf{T}]\{\dot{\mathbf{u}}\} + \{\mathbf{F}\}_0 \tag{14}$$

is obtained, where $[\mathbf{U}]$, $[\mathbf{T}]$ are matrices assembled from element contributions (Equation (13)) and $\{\mathbf{t}\}$, $\{\dot{\mathbf{u}}\}$ are vectors that collect all traction and velocity components on

points $\mathbf{y}_n$. $\{\mathbf{F}\}_0$ relates to the integrals involving body forces. Either $\mathbf{t}$ or $\dot{\mathbf{u}}$ must be known on the boundary, so for a mixed boundary value problem we have

$$[\mathbf{L}]\{\mathbf{a}\} = \{\mathbf{F}\} + \{\mathbf{F}\}_0 \tag{15}$$

where $[\mathbf{L}]$ contains a mixture of $[\mathbf{U}]$,$[\mathbf{T}]$ coefficients and $\{\mathbf{a}\}$ contains a mixture of unknown tractions and velocities. $\{\mathbf{F}\}_0$ is a vector computed with known boundary values.

3.2 Results in the domain

The solution algorithm requires the evaluation of the perturbation velocities inside the domain V_0. The velocity vector $\mathbf{v}$[1] at any internal point $\mathbf{y}_i$ can be computed by

$$\mathbf{v}(\mathbf{y}_i) = \int_S \mathbf{U}(\mathbf{y}_i, \mathbf{x})\,\mathbf{t}(\mathbf{x})\,\mathrm{d}S - \int_S \mathbf{T}(\mathbf{y}_i, \mathbf{x})\,\dot{\mathbf{u}}(\mathbf{x})\,\mathrm{d}S \tag{16}$$
$$- \int_{S_0} \mathbf{U}(\mathbf{y}_i, \bar{\mathbf{x}})\,\mathbf{b}_0(\mathbf{x})\,\mathbf{n}(\mathbf{x})\,\mathrm{d}S_0 + \int_{V_0} \mathbf{U}'(\mathbf{y}_i, \bar{\mathbf{x}})\,\mathbf{b}_0(\bar{\mathbf{x}})\,\mathrm{d}V_0$$

After inserting the approximations for $\dot{\mathbf{u}}$, $\mathbf{t}$ and $\mathbf{b}_0$ the equation above can be written in matrix notation as:

$$\{\mathbf{v}\} = [\mathbf{A}]\,\{\mathbf{t}\} - [\mathbf{C}]\,\{\dot{\mathbf{u}}\} + [\mathbf{D}]\,\{\mathbf{b}_0\} \tag{17}$$

where matrices $[\mathbf{A}]$ and $[\mathbf{C}]$ are assembled from element contributions of Kernel basis function products and $[\mathbf{D}] = \left([\mathbf{D}]^V - [\mathbf{D}]^S\right)$.

3.3 Iterative procedure - Modified Newton-Raphson

There are two possibilities for the iterative procedure: modified Newton-Raphson or full Newton-Raphson. In the former the left hand side of the system of equations is not changed and only a new right hand side is computed at each iteration, whereas in the latter the left hand side is changed at every iteration. The test examples is a pure Dirichlet problem, i.e. $\{\mathbf{a}\} = \{\mathbf{t}\}$ in Equation (15) and therefore the unknown are boundary tractions $\{\mathbf{t}\}$ and the known values are perturbation velocities $\{\dot{\mathbf{u}}\}$ at the boundary. Without loss of generality, the algorithms are detailed for this special case as the extension to mixed boundary conditions is trivial. The iterative procedure for modified Newton-Raphson is essentially the same as used in [5] and described in more detail in [6]. For the first iteration the unknowns are computed by

$$[\mathbf{U}]\{\mathbf{t}\}^0 = \{\mathbf{F}\} \tag{18}$$

For the subsequent iteration we have

$$[\mathbf{U}]\{\mathbf{t}\}^k = \{\mathbf{F}\} + \{\mathbf{F}\}_0^{k-1} \tag{19}$$

[1] The velocities at internal points are referred to as $\mathbf{v}$ to distinguish them from the boundary velocities $\dot{\mathbf{u}}$.

where k is an iteration counter. The velocities at internal points are computed by:

$$\{\mathbf{v}\}^0 = [\mathbf{A}]\ \{\mathbf{t}\}^0 - [\mathbf{C}]\ \{\dot{\mathbf{u}}\} \tag{20}$$

for the first iteration and

$$\{\mathbf{v}\}^k = [\mathbf{A}]\ \{\mathbf{t}\} - [\mathbf{C}]\ \{\dot{\mathbf{u}}\} + [\mathbf{D}]\ \{\mathbf{b}_0\} \tag{21}$$

for the subsequent iterations. To ensure convergence for higher Reynolds numbers we apply a relaxation scheme, i.e. the tractions and velocities are computed by a combination of new and previous values, where β is a relaxation coefficient ($0 < \beta < 1$):

$$\begin{aligned} \{\mathbf{t}\} &= \beta\,\{\mathbf{t}\}^k + (1-\beta)\,\{\mathbf{t}\}^{k-1} \\ \{\mathbf{v}\} &= \beta\,\{\mathbf{v}\}^k + (1-\beta)\,\{\mathbf{v}\}^{k-1} \end{aligned} \tag{22}$$

3.4 Numerical results - Isoparametric discretisation

The implementation of the theory is tested here on the standard problem of a driven cavity. The results are compared with an available fine grained solution of [1] in order to ascertain that good quality of results can be obtained. An incompressible fluid of uniform viscosity ($\mu = 1$) is confined within a square region of dimension $H = 1 \times 1$. The fluid velocities on the bottom, left and right are fixed at zero, while a uniform velocity $u_x = 1$ is specified at the top, which is tapered off to zero very near the corners. The Reynolds number is defined as $Re = \rho\, U\, H/\mu$. The example is tested for different Reynolds numbers by changing the value of ρ.

3.4.1 Definition of geometry

The boundary of the problem is defined by either linear or quadratic boundary elements. The element lengths are graded towards the edges of the cavity. As shown in Figure 1 three mesh densities are considered with 10, 20 and 30 elements along each edge of the cavity. The volume of the domain is discretised with cells with basis functions of

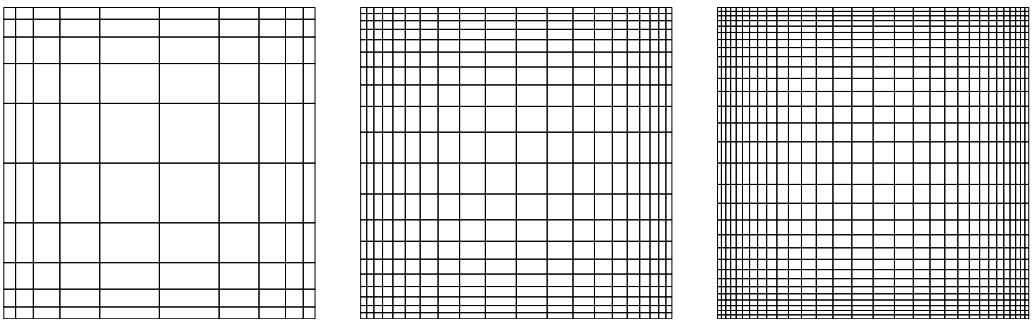

Figure 1: Definition of Geometry with 10, 20 and 30 boundary elements at each edge of the cavity

either linear or quadratic order, describing the geometry and the velocity in the interior. In Table 1 the number of degrees of freedom associated to the nodes at the boundary and the number of internal points are shown for the three meshes and the reference solution of [1].

Table 1: Mesh statistics

Mesh	Degrees of freedom	No. of internal points
10 linear	80	81
10 quadratic	160	261
20 linear	160	361
20 quadratic	320	1121
30 linear	240	841
30 quadratic	480	2581
Reference [1]	-	16641

3.4.2 Results and comparison

Results were computed for the three meshes with linear and quadratic elements for Reynolds numbers 100, 200 and 300 with a modified Newton-Raphson method with relaxation. Figure 2 shows the velocity vectors for Reynolds numbers 0 and 300. A shift in the vortex centre can be clearly seen. Figures 3, 4 and 5 show a comparison of the results obtained for the different meshes. For Reynolds number 100 the variation of x-velocities along a vertical line through the middle for all meshes agree well with the extremely accurate published solution. For the results with Reynolds number 200 and 300 no reference solutions were available. But, as shown in Figure 4 for Reynolds number 200 the results of the different meshes agree well, even for the course meshes. The results for Reynolds number 300 (Figure 5) deviate from each other. With the modified Newton-Raphson iterativie algorithm with relaxation a solution was difficult to achieve and for higher Reynolds numbers no converged results could be obtained.

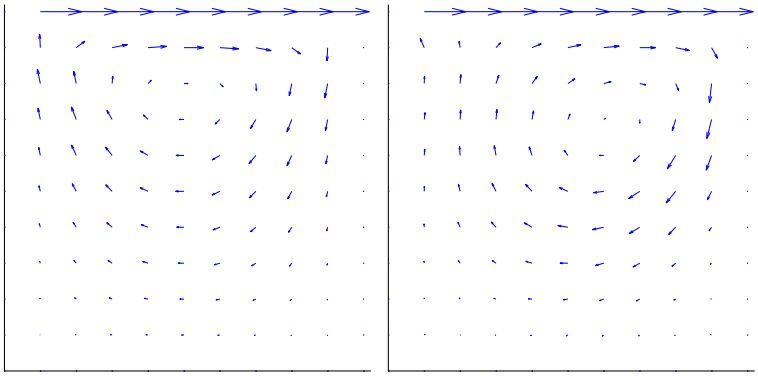

Figure 2: Forced cavity flow: Resulting velocity vectors for Re=0 and Re=300

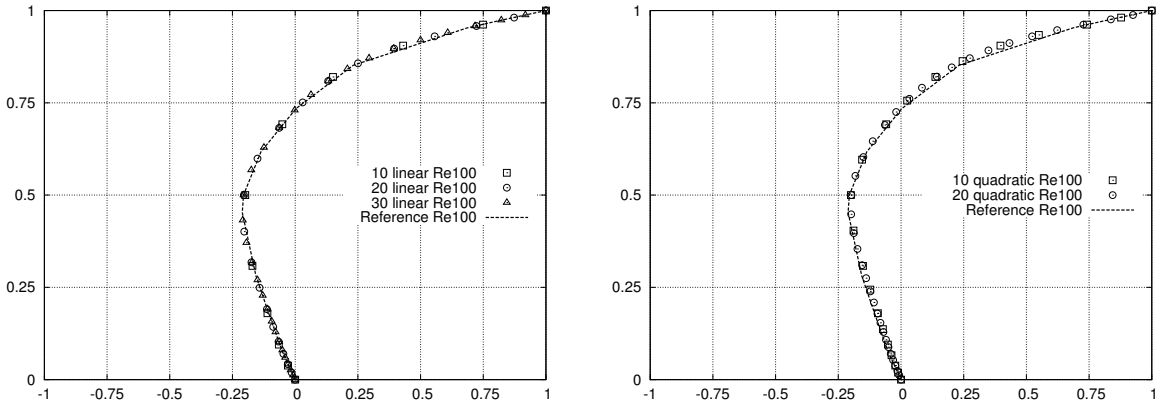

Figure 3: Comparison of velocity in x-direction along a vertical line through centre for Re=100 for linear (left) and quadratic elements (right) together with the reference solution

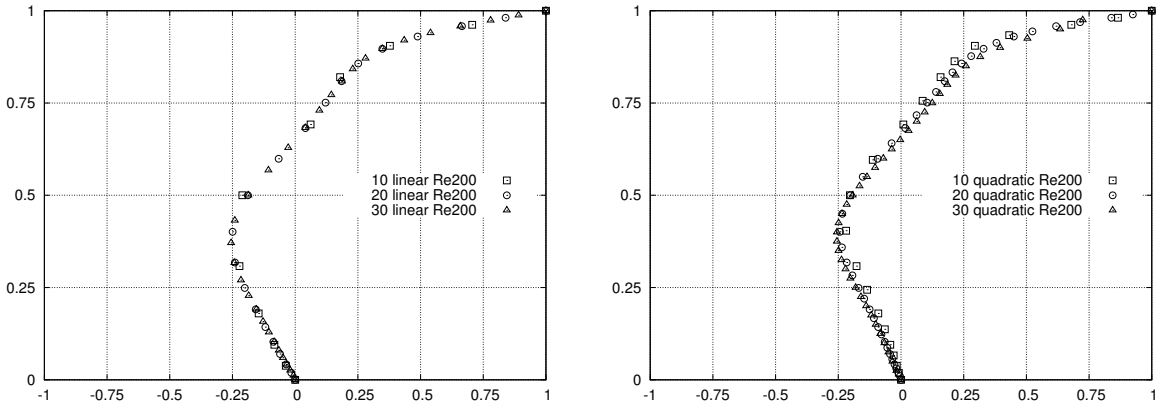

Figure 4: Comparison of velocity in x-direction along a vertical line through centre for Re=200 for linear (left) and quadratic elements (right)

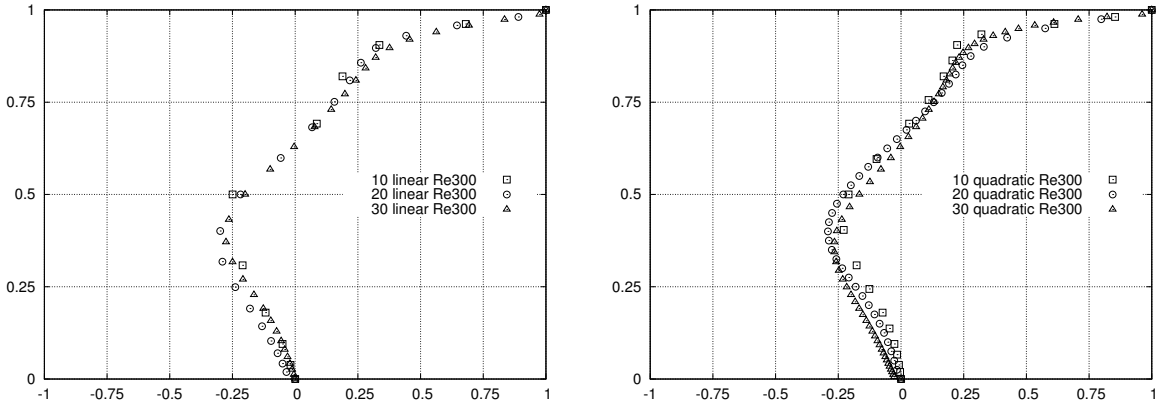

Figure 5: Comparison of velocity in x-direction along a vertical line through centre for Re=300 for linear (left) and quadratic elements (right)

4 ISOGEOMETRIC DISCRETISATION

For the discretisation of the surface integrals over the boundary S of Equation (10) and Equation (12) the boundary is divided into patches and a geometry independent field approximation approach is adopted for each patch, i.e. different basis functions for the description of the geometry and for the field values are used.

$$\mathbf{x}^e = \sum_{k=1}^{K} R_k(s)\,\mathbf{x}_k^e \qquad \dot{\mathbf{u}}^e = \sum_{k=1}^{K^u} R_k^u(s)\,\dot{\mathbf{u}}_k^e \qquad \mathbf{t}^e = \sum_{k=1}^{K^t} R_k^t(s)\,\mathbf{t}_k^e \tag{23}$$

In the above equations the superscript e refers to the number of the patch, R_k, R_k^u and R_k^t are NURBS basis functions with respect to the local coordinate s for the geometry, velocities and tractions respectively. $\mathbf{x}_k^e$ specify the location of control points and $\dot{\mathbf{u}}_k^e$ and $\mathbf{t}_k^e$ are the parameters for velocities and tractions. K, K^u, K^t are the number of parameters for each patch. The advantage of using NURBS is that they are much better suited than Lagrange polynomials for describing smooth boundaries and that superior refinement strategies such as order elevation, knot insertion and k-refinement, can be used. By manipulating the knot vector one can easily influence the continuity of the basis functions for the approximation of unknown values. Inserting the approximations into the integral equations the same final equation system arise as shown in Equation (15). For the evaluation of the domain integral the domain V_0 is described by a mapping method introduced recently for 2D in [7] and extended to 3D in [8]. In this approach the domain is defined by two NURBS curves and a linear interpolation between them as shown in the Figure 6. A detailed description of the evaluation of the volume integral has been recently submitted by Beer et al. [6].

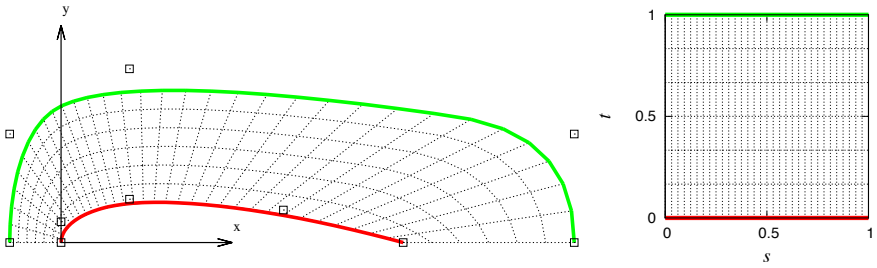

Figure 6: Example of definition of volume V_0 surrounding half of an airfoil in (left) global x,y and (right) local s,t coordinate system. The red curve defines the boundary of the airfoil as well as the bottom boundary of the domain V_0. The green curve defines its top boundary. The associated control points are depicted by hollow squares. Note that only 5 control points are required to accurately define the shape of the airfoil and 5 more control points the surrounding domain.

4.1 Iterative procedure

Additionally to the the modified Newton-Raphson with a relaxation scheme described in section 3.3 a full Newton-Raphson is implemented in the NURBS based code. With this the left hand side of Equation (15) is modified at each iteration. The theory and implementation is described in [6].

4.2 Numerical results - Isogeometric discretisation

For the described driven cavity problem of section 3.4 the boundary is defined by 4 linear NURBS patches. The approximation of the boundary unknown was achieved by inserting knots and by order elevating the basis functions for describing the geometry (from linear to quadratic). Three different refinements were investigated and the resulting locations of collocation points computed using Greville abscissa [9] are shown in Figure 7.

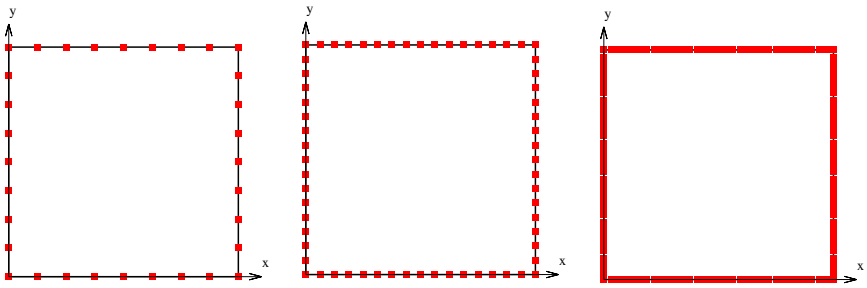

Figure 7: Refinement of solution: Location of collocation points for 3, 7 and 15 knot insertions for each patch

The domain for the volume integration was defined by 2 NURBS curves. The refinement of the boundary values was accompanied by an increased number of internal points as shown in Figure 8. Quadratic interpolation between the points was assumed.

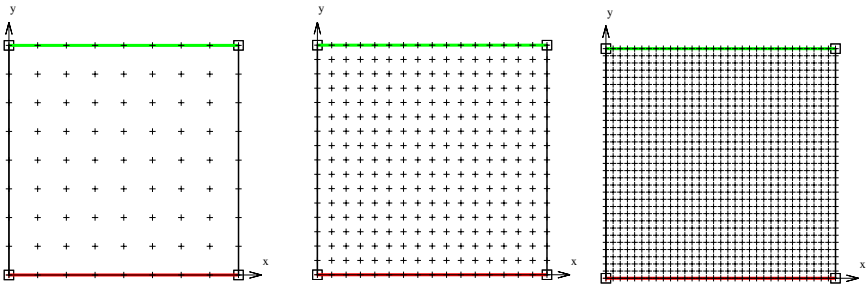

Figure 8: Definition of domain for volume integration with two NURBS curves marked red and green and location of the internal points for the three refinement stages

The number of degrees of freedom and the number of internal points for the different meshes is shown in Table 2.

Table 2: Mesh statistics

Mesh	Degrees of freedom	No. of internal points
mesh1	64	81
mesh2	128	289
mesh3	256	1089
Reference [1]	-	16641

Compared to the isoparametric results with the isogeometric approach a solution for Reynolds number Re=400 with the modified Newton-Raphson as well as with the full Newton-Raphson iteration is possible. There is very little difference between the results obtained with modified and full Newton-Raphson as shown in Figure 9. However, as shown in Table 3 there is a large difference with respect to the number of iterations required to achieve convergence to a tolerance of 10^{-4} with the modified Newton-Raphson requiring a significant higher number of iterations.

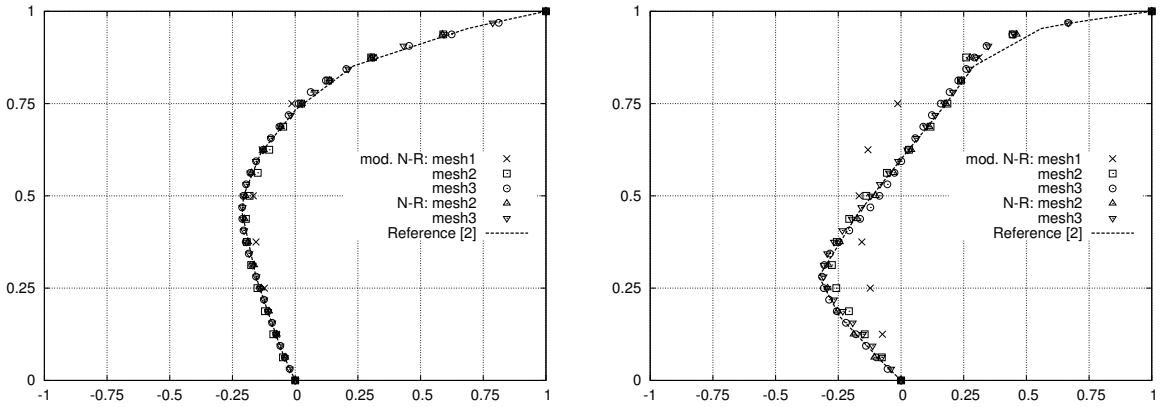

Figure 9: Comparison of velocity in x-direction along a vertical line through centre for Re=100 (left) and Re=400 (right) together with the reference solution

Table 3: Number of iterations required for convergence

		mesh 1	mesh 2	mesh3
Re=100	modified Newton-Raphson	15	19	18
	full Newton-Raphson	3	3	3
Re=400	modified Newton-Raphson	24	39	100
	full Newton-Raphson	-	5	5

5 Conclusion

A comparison of isoparametric and isogeometric BEM discretisation is shown for the benchmark example of the driven cavity problem in 2D. Excellent results for moderate Reynolds numbers could be obtained for both discretisation methods even for coarse meshes. For increasing Reynolds numbers it seems that isogeometric discretisation leads to a better convergence behaviour then isoparametric discretisation. With respect to iterative techniques a full Newton-Raphson method is necessary to achieve results for higher Reynolds numbers with a moderate number of iterations.

REFERENCES

[1] U. Ghia, K. N. Ghia, C. T. Shin, High-Re Solutions for incompressible flow using the Navier-Stokes equations and Multigrid Method, Journal of computational physics 48 (1982) 387–411.

[2] G. Beer, Advanced numerical simulation methods - From CAD Data directly to simulation results, CRC Press/Balkema, 2015.

[3] T. Hughes, J. Cottrell, Y. Bazilevs, Isogeometric analysis: CAD, finite elements, NURBS, exact geometry and mesh refinement, Computer Methods in Applied Mechanics and Engineering 194 (39–41) (2005) 4135–4195.

[4] G. Dargush, P. Banerjee, Boundary Element Methods in Nonlinear Fluid Dynamics, Vol. 6 of Developments in boundary element methods, Elsevier, 1990, Ch. Advanced boundary element methods for steady incompressible thermoviscous flow.

[5] M. Aydin, R. T. Fenner, Boundary element analysis of driven cavity flow for low and moderate Reynolds numbers, International Journal for Numerical Methods in Fluids 37 (2000) 45–64.

[6] G. Beer, V. Mallardo, E. Ruocco, C. Duenser, Isogeometric boundary element analysis of steady incompressible viscous flow, part 1: plane problems, Computer Methods in Applied Mechanics and Engineering submitted February 2017.

[7] G. Beer, B. Marussig, J. Zechner, C. Duenser, T.-P. Fries, Isogeometric boundary element analysis with elasto-plastic inclusions. part 1: plane problems, Computer Methods in Applied Mechanics and Engineering 308 (2016) 552–570.

[8] G. Beer, V. Mallardo, E. Ruocco, B. Marussig, J. Zechner, C. Duenser, T. P. Fries, Isogeometric boundary element analysis with elasto-plastic inclusions. part 2: 3-d problems, Computer Methods in Applied Mechanics and Engineering 315 (2017) 418–433.

[9] R. W. Johnson, Higher order B-spline collocation at the Greville abscissae, Applied Numerical Mathematics 52 (1) (2005) 63 – 75.